iet

Design and calibration method for precise temperature sensor

Kamil Stepniewski, Bartosz Dec, Arkadiusz Łuczyk, Jakub Jasiński, and Krzysztof Siwiec

Abstract—This paper presents the design of the temperature sensor and analysis of different calibration methods. The main aspect of the analysis was optimization of the number and location of the measurement points needed to perform the calibration for a given accuracy. For this purpose, temperature sensors using proportional to the absolute temperature (PTAT) current and current controlled oscillator (CCO) have been designed in 180 nm technology. To reduce the sensitivity of the sensor to the supply voltage, the low dropout regulator (LDO) has been used. The bandgap circuit generates the stable reference voltage for the LDO and PTAT current for the CCO

Keywords—temperature Sensor, bandgap reference voltage, voltage regulator, current-controlled oscillator, polynomial calibration

I. Introduction

NTEGRATED circuits, owing to their compact dimensions, have dominated the modern electronics market. Today's technology enables the fabrication of transistors with characteristic dimensions of just a few nanometers, allowing for the design of multifunctional circuits within footprints of only few square millimeters. Additional advantages of integrated circuits include low power consumption and high reliability. The presented work has been conducted as part of the development of a cryptographic processor compliant with the Common Criteria standard. It specifically focuses on a temperature sensor circuit designed to monitor the operating conditions of the cryptographic system and prevent side-channel attacks.

Temperature has a significant impact on the electrical parameters of both passive and active components in CMOS circuits, which can lead to malfunctions in their proper operation. For example, an increase in temperature reduces the mobility of charge carriers in the transistor channel (μ_n and μ_p), leading to a decrease in the drain current I_{DS} and thus prolonging switching times. Additionally, the resistance of passive elements and interconnects increase with temperature rise, which can change operating points.

Parasitic capacitances (such as gate-to-substrate capacitance) also vary due to the temperature dependence of dielectric permittivity, affecting the circuit's operating frequency

This work was supported in part by the Polish National Center for Research and Development under project No. CYBERSECI-DENT/369203/I/NCBR/2017.

of Authors are with the Institute Microelectronics and Technology, Optoelectronics, Warsaw University of (e-mail: kamil.stepniewski@pw.edu.pl, tosz.dec@pw.edu.pl, arkadiusz.luczyk@pw.edu.pl, jakub.jasinski@pw.edu.pl, krzysztof.siwiec@pw.edu.pl)

and stability. A temperature sensor allows not only detecting physical attacks, such as localized overheating or point cooling (e.g., using liquid nitrogen), but also can help with dynamic compensation of parameter changes.

The designed sensor utilizes a proportional to absolute temperature (PTAT) current to bias a ring oscillator (OSC). The temperature of the integrated circuit is determined based on frequency measurement. A bandgap reference circuit (BGR) was used as the source of the PTAT current. An internal supply voltage for the OSC was designed to reduce the influence of power supply variations on the temperature measurement. A low-dropout (LDO) voltage regulator was used, with the reference voltage (VREF) from the BGR supplied to its input. The sensor was fabricated using X-FAB's 180 nm CMOS technology. A significant aspect of this work was the analysis and optimization of the sensor calibration process. Polynomial extrapolation of the sensor's characteristic was chosen. The influence of the polynomial degree was analyzed, and the selection of measurement points were optimized.

II. DESIGN OF TEMPERATURE SENSOR

The chapter presents the design of the temperature sensor. Figure 1 illustrates the high-level architecture of the system. In the designed temperature sensor, a Bandgap Reference (BGR) circuit was used to generate a proportional to the absolute temperature (PTAT) current. This PTAT current biases the Current-Controlled Oscillator (CCO) generator, producing a clock signal whose frequency is proportional to the temperature. The frequency of the generated signal is measured to determine the current temperature of the integrated circuit.

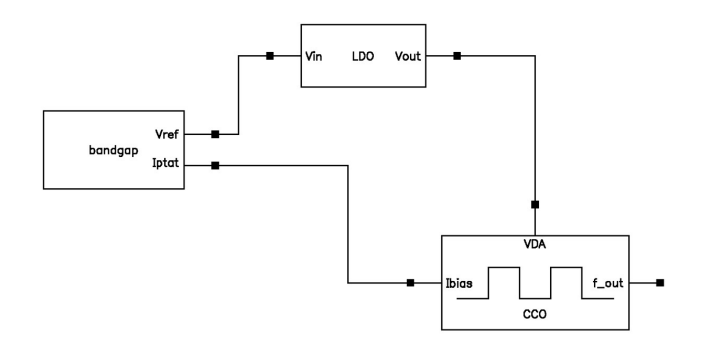


Fig. 1. Architecture of Temperature Sensor.



To minimize the impact of supply voltage variations on the accuracy of the temperature measurement, an internal regulated supply was implemented. A Low-Dropout Regulator (LDO) was utilized, with the reference voltage (VREF) provided by BGR circuit.

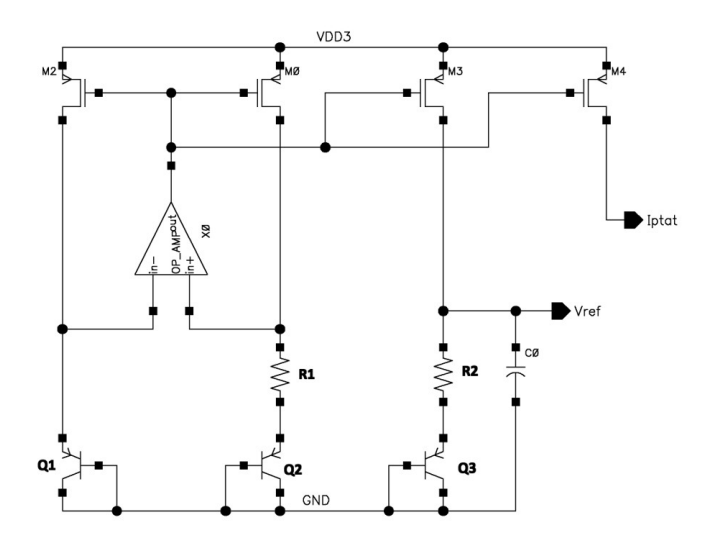


Fig. 2. Bandgap Reference Voltage circuit schematic.

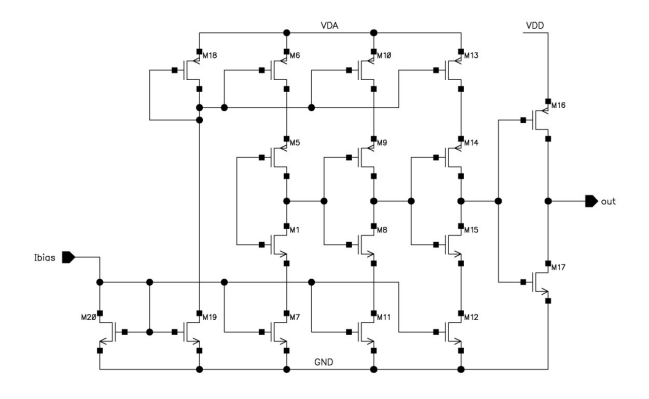


Fig. 3. Electrical schematic of Ring Oscillator.

III. BANDGAP VOLTAGE REFERENCE CIRCUIT

The temperature sensor design utilizes BGR circuit, which generates the reference voltage using a PTAT current. An additional BGR's current output is used to bias OSC, while the reference voltage serves as the input signal for LDO. An operational amplifier and capacitor on V_{REF} reduce supply voltage effect on the circuit. The schematic is presented in Figure 2. The biasing current of CCO can be calculated using Equation 1 [1]. The reference voltage is the sum of voltage across a resistor and base-emitter voltage of PNP transistor (Equation 2 [1]).

$$I_{PTAT} = \frac{k * ln(K)}{q * R_1} * T \tag{1}$$

$$U_{REF} = I_{PTAT} * R_2 * U_{BE3} \tag{2}$$

Where:

- k Boltzman constant
- q Elementary charge
- K Ratio of bipolar transistor count $(\frac{Q2}{Q1})$
- \bullet T Temperature
- \bullet R_1 and R_2 Resistances on BGR schematic
- U_{BE3} Base-emitter voltage of transistor Q3

IV. RING OSCILLATOR

Ring oscillator generates clock signal whose frequency is proportional to the value of the bias current. A current-starved oscillator architecture was chosen, consisting of series of three inverters connected in a feedback loop. The schematic of the oscillator is shown in Figure 3. The oscillation frequency can be calculated using Equation 3 [1]. Last stage of the circuit is a buffer, that converts the sinusoidal waveform into a square clock signal.

$$f_{osc} = \frac{I_{BIAS}}{N * V_{DD} * C_{tot}} \tag{3}$$

Where:

- I_{BIAS} Oscillator biasing current
- N Number of Inverters in the feedback loop
- ullet V_{DD} Supply voltage for oscillating part
- C_{tot} Total capacitance between individual inverters (sum of output capacitance of previous stage and input capacitance of next stage)

V. VOLTAGE REGULATOR

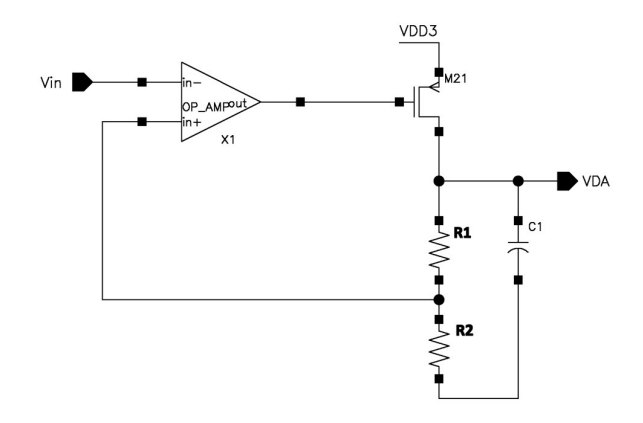


Fig. 4. Electrical schematic of Voltage Regulator.

A voltage regulator was used to provide stable supply voltage for the oscillator. The input to the regulator input is reference voltage generated by the BGR, ensuring that the internal supply remains stable across temperature variations. The schematic is shown in Figure 4, while its output voltage is given by Equation 4 [1].

$$VDA = V_{in} * \frac{R_1 + R_2}{R_2} \tag{4}$$

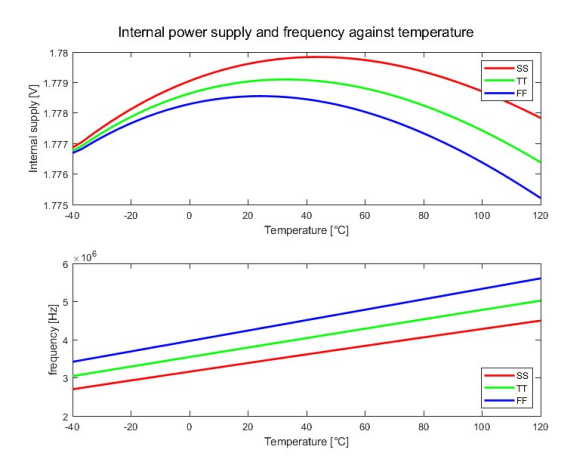


Fig. 5. Internal power supply and frequency against temperature.

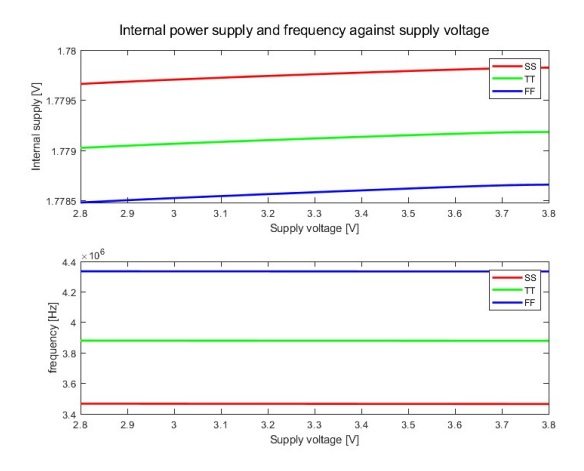


Fig. 6. Internal power supply and frequency against supply voltage.

VI. SIMULATION OF TEMPERATURE SENSOR

Post-layout simulations were performed using process corner analysis. The SS, SF, TT, FS and FF corner models were considered. Simulation results for the internal supply voltage and the oscillator frequency, as a function of temperature and main supply voltage, are presented in Figure 5 and 6, respectively. Table I summarizes the simulation results for the process corner analysis.

The internal power supply as a function of temperature and main supply voltage remains stable. The relationship between output frequency and temperature is close to linear. On the other hand, temperature sensor has low main supply voltage dependence, 1 V change leads to approximately 0.2°C error. The difference between FF and SS corner is a result of resistance corner models, which leads to change of operating points in BGR.

VII. CALIBRATION OF TEMPERATURE SENSOR

The obtained curves of the sensor's output frequency as a function of temperature are nonlinear. The shape of the curve depends on the manufacturing process. To achieve satisfactory measurement accuracy, post-production calibration will be necessary.

TABLE I SIMULATION RESULTS FOR CORNER SIMULATIONS.

	SS	TT	FF
$VDA@(T = 27^{\circ}C, V_{DD} = 3.3V)[V]$	1.779	1.779	1.779
$VDA[ppm/^{\circ}C]$	9.55	10.42	11.76
$VDA[\mu V/V]$	158	162	178
$f_{out}@(T = 27^{\circ}C, V_{DD} = 3.3V)[MHz]$	3.501	3.917	4.367
$f_{out}[\mathrm{KHz}/^{\circ}\mathrm{C}]$	11.24	12.37	13.68
$f_{out}[{ m KHz/V}]$	1.867	1.459	1.190
$I_{SUPPLY}@(T = 27^{\circ}C, V_{DD} = 3.3V)[\mu A]$	62	76	93
$t_{START}[\mathrm{ms}]$	0.59	0.24	0.06

The operating temperature of the integrated circuit will be determined by measuring the frequency and referencing the corresponding temperature from the curve. An extrapolated frequency-versus-temperature curve will be determined based on measurement points.

The main aspect of calibration was achieving precise measurement accuracy, while optimizing the time spent on calibration. In the search for an optimal solution, polynomials of degrees 1 through 4 were tested for extrapolation. The number of required measurement points depends on the polynomial degree used. Alternately cooling and heating the integrated circuits is a time-consuming process. Therefore, the relationship between the temperature range from which measurement points were collected and the accuracy of temperature measurement was investigated. The effect of quantization was also tested.

The calibration process was evaluated using simulation results. Simulations were performed for temperatures ranging from -40°C to 120°C with a 5°C step. Monte Carlo analysis was applied, incorporating both global and local variations. A total of 200 simulations were run, and the standard deviation was set to 3σ . The simulation results are presented in Figure 7. A MATLAB script was developed to plot the curve for a given configuration of measurement points. For polynomials of degree 3 and higher, the frequency at room temperature was included as one of the measurement points. The resulting characteristic was compared with the simulation results, and the temperature reading error was calculated based on the difference. The above procedure was repeated for all measurement point configurations, and then those yielding the smallest error for the specified range were selected.

Figure 8 shows the results of the average and maximum calibration errors as a function of the temperature range from which the measurement points were chosen. It can be seen that to exploit the benefits of using higher order polynomial, much larger temperature range has to be used for calibration. From the practical point of view second order polynomial seems to be the most optimal choice.

Using a second-degree polynomial for characteristic extrapolation yields the best results, as it achieves small calibration errors with a relatively narrow temperature range. A first-degree polynomial may be used if low accuracy is acceptable or if the temperature sensor is intended for a smaller temperature range. While third- and fourth-degree polynomials offer slight improvements over the second-degree polynomial, they

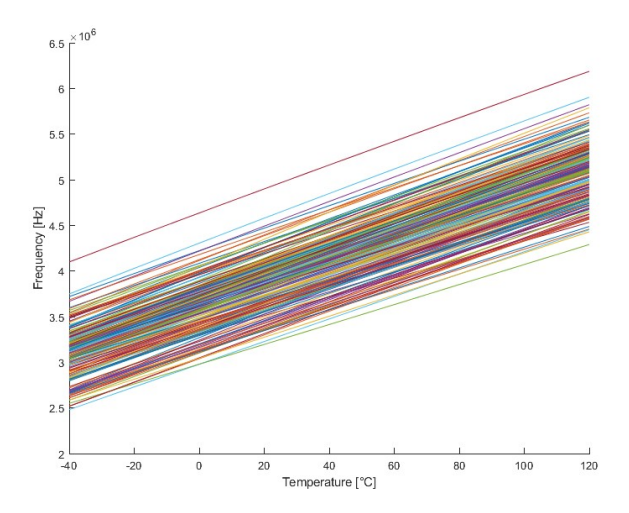


Fig. 7. Frequency in function of temperature in random simulation.

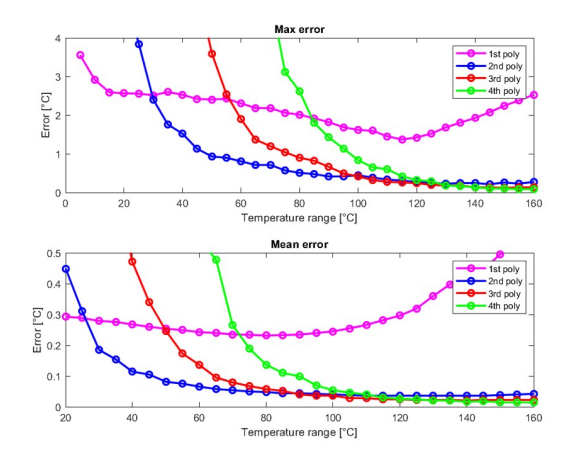


Fig. 8. Calibration results for different polynomial stages.

come at the cost of requiring an larger range of measurement points, consequently extending the calibration process.

The lowest calibration error with max error 0.16°C was achieved for measurement points: -25°C, 27°C and 110°C. The effect of quantization of output frequency and polynomial coefficient was tested. Figure 9 presents the calibration results for two hundred simulations seen in Figure 7. It can be seen that the maximum error is kept below 0.16°C and in most cases is even close to and 0.1°C. The impact of the coefficients quantization was also verified (see 10). It can be seen that for 12-bits the results are decent and the difference between using 13 and 14 bits is minor.

The analysis of the temperature sensor calibration can be summarized as follows:

- First-degree polynomial extrapolation results significant errors due to the parabolic shape of the characteristic curve.
- Third- and fourth-degree polynomials offer only minor improvement compared to the second-degree polynomial.
- Expanding the range from which measurement points are collected leads to a reduction in calibration error.

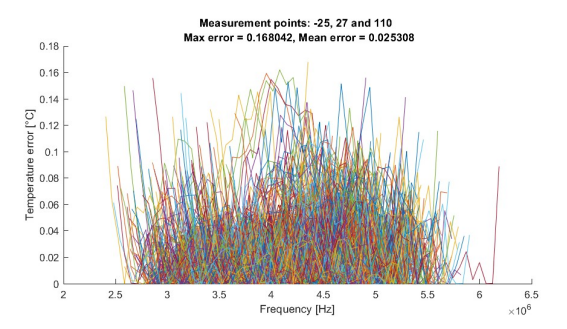


Fig. 9. Calibration results for 2nd stage polynomial.

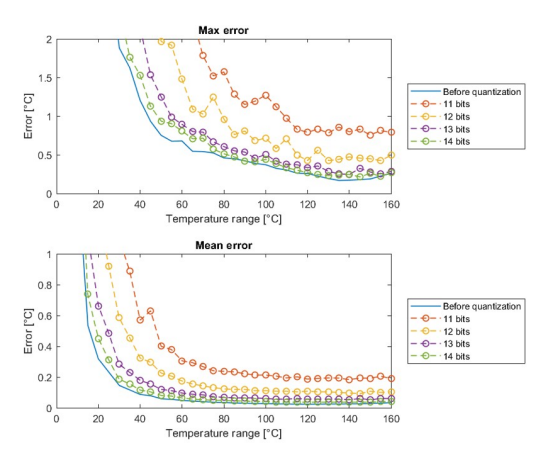


Fig. 10. Quantization effect on temperature error for 2nd stage polynomial.

- Higher-degree polynomials require a larger range of measurement points.
- The error versus temperature range plot shows a point beyond which further increasing the range results in only a negligible improvement in accuracy.

VIII. CALIBRATION OF TEMPERATURE SENSOR IN HHGRACE TECHNOLOGY

To ensure the reliability and accuracy of the temperature sensor's calibration, it is essential to test the calibration process in a different CMOS technology. Variations in process parameters such as threshold voltage, oxide thickness, and doping concentrations can significantly affect the behavior of temperature-dependent circuits. Therefore, a calibration method that performs well in one technology node may not yield accurate results in another without modification. By validating the calibration process in different technology, we can assess its robustness and potential for reuse in similar designs.

The temperature sensor in HHGrace 90 nm technology was designed. Post-layout simulations were performed using process corner analysis. Simulation results for the internal supply voltage and the oscillator frequency, as a function of temperature and main supply voltage, are presented in Figure 11 and 12, respectively. Table II summarizes the simulation results for the process corner analysis. Monte Carlo analysis with the same parameters as in X-FAB technology was performed, whose result is shown in Figure 13. Figure 14, 15 and

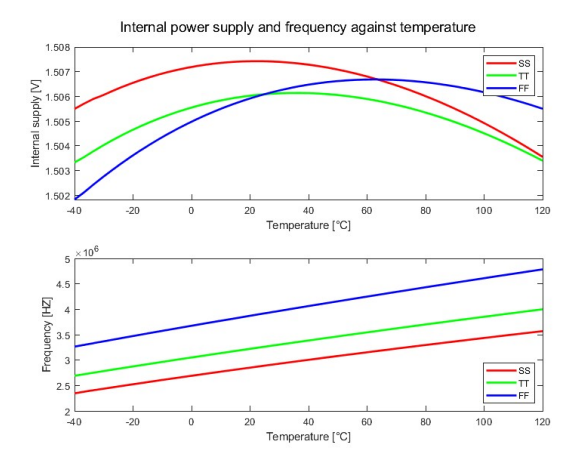


Fig. 11. Internal power supply and frequency against temperature - HHGrace.

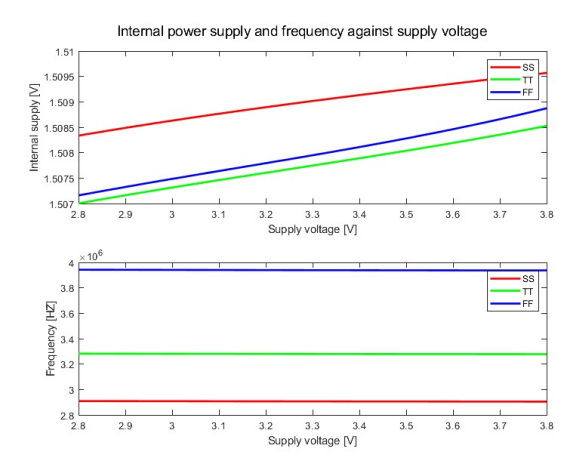


Fig. 12. Internal power supply and frequency against supply voltage - HHGrace.

16 presents calibration results for different polynomial stages, calibration results for 2nd stage polynomial and quantization error respectively for temperature sensor designed in HHGrace technology. It can be seen that the character of all of the curves is similar to that observed for X-FAB technology. It matches expectations as although parameters such as voltage threshold or carrier mobility can differ, the physics of the device remains the same. Due to that fact the calibration method is still valid and allows to achieve similar results with respect to the accuracy.

MATLAB script found 29 configurations of measurement points, where maximum extrapolation error is below 0.3°C. The 1st measurement point is chosen from temperature ranging from -40°C to -25°C, 3rd is chosen from 95° to 120°C (2nd is always 27°C). Similar results were achieved for temperature sensor designed for X-FAB technology. There are 30 configurations, where 1st measurement point from -40°C, to -15°C and 2nd from 95°C to 120°C. The optimum calibration points might be vary for each technology, but the difference between the best configuration and 30th is around 0.1°C. If the best possible accuracy is expected, the measurement points should be chosen individually for each temperature sensor.

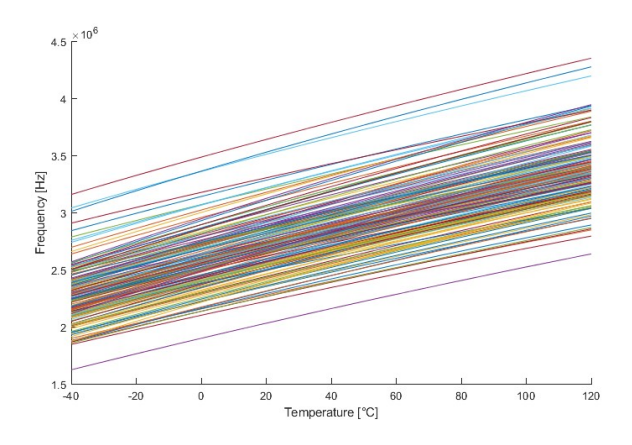


Fig. 13. Frequency in function of temperature in random simulation - HHGrace.

TABLE II SIMULATION RESULTS FOR CORNER SIMULATIONS - HHGRACE.

	SS	TT	FF
$VDA@(T=27^{\circ}\mathrm{C},V_{DD}=3.3\mathrm{V})[\mathrm{V}]$	1.507	1.506	1.506
$VDA[ppm/^{\circ}C]$	16.08	11.69	20.20
$VDA[\mu V/V]$	1234	1524	1714
$f_{out}@(T = 27^{\circ}\text{C}, V_{DD} = 3.3\text{V})[\text{MHz}]$	2.907	3.280	3.939
$f_{out}[\mathrm{kHz}/^{\circ}\mathrm{C}]$	7.650	8.176	9.502
$f_{out}[\mathrm{kHz/V}]$	4.146	4.575	5.506
$I_{SUPPLY}@(T = 27^{\circ}\text{C}, V_{DD} = 3.3\text{V})[\mu\text{A}]$	26	32	41
$t_{START}[\mu \mathrm{s}]$	20	8	4

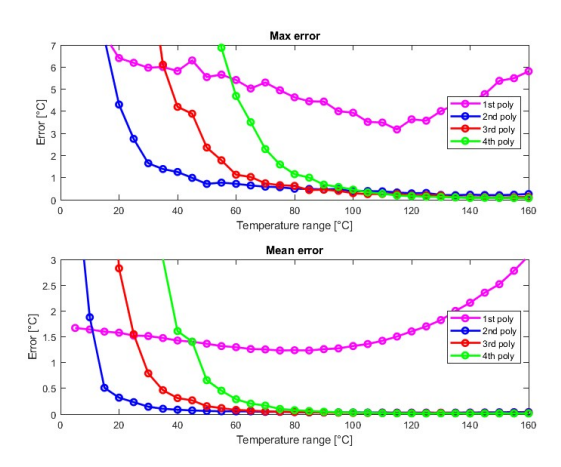


Fig. 14. Calibration results for different polynomial stages - HHGrace.

IX. MEASUREMENT OF MANUFACTURED TEMPERATURE SENSOR

Measurements were conducted in a climatic chamber, which allowed temperature control within the range of -35°C to 120°C. The frequency was measured using an oscilloscope, while the internal supply voltage was measured with a multimeter. The measurement results for both the internal supply voltage and the sensor's output frequency as a function of temperature are displayed in Figure 17. Optimal measurement

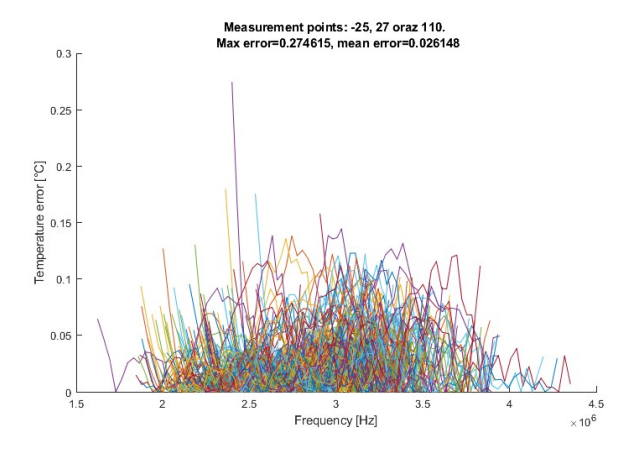


Fig. 15. Calibration results for 2nd stage polynomial - HHGrace.

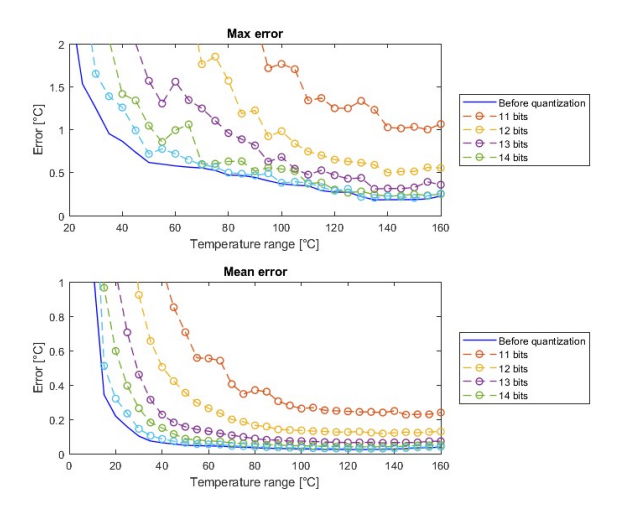


Fig. 16. Quantization effect on temperature error for 2nd stage polynomial - HHGrace.

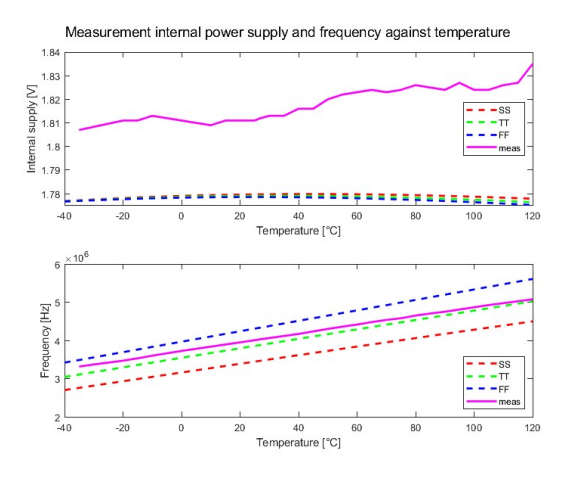


Fig. 17. Measurement results as function of temperature.

points (-25°C, 27°C, 110°C) were selected to calculate polynomial coefficients. Then the polynomial curve was compared with measurement points, and the resulting measurement error was calculated. The polynomial curve is shown in Figure 18, while measurement error is presented in Figure 19.

Figure 20 illustrates measurement board with the manufactured integrated circuit mounted at the center. The temperature sensor was fabricated using X-FAB 180 nm CMOS technology. The layout of the production masks is shown in Figure 21, with closer look at temperature sensor in Figure 22. The temperature sensor's footprint is 330 μ m by 123 μ m.

X. SUMMARY

This paper presents the design, simulations, and post-fabrication measurements of the temperature sensor. The designed circuit was fabricated using X-FAB 180 nm CMOS technology. A special polynomial extrapolation calibration method was used and analyzed, incorporating optimization techniques to achieve higher measurement accuracy and reduce the time spent on calibration. To validate the method,

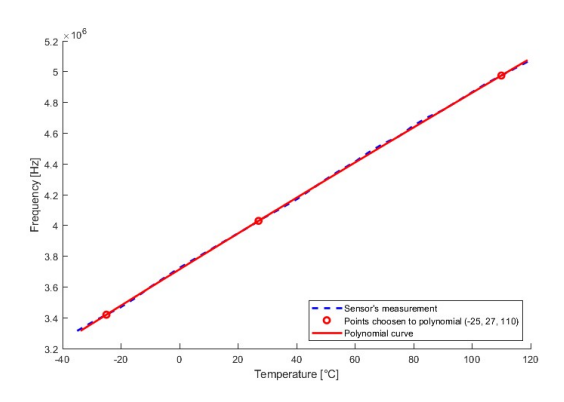


Fig. 18. Polynomial curve from selected measurement points.

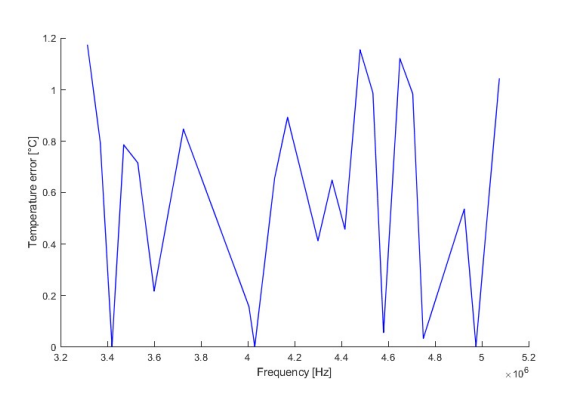


Fig. 19. Calibration process error.



Fig. 20. Temperature sensor testing board.

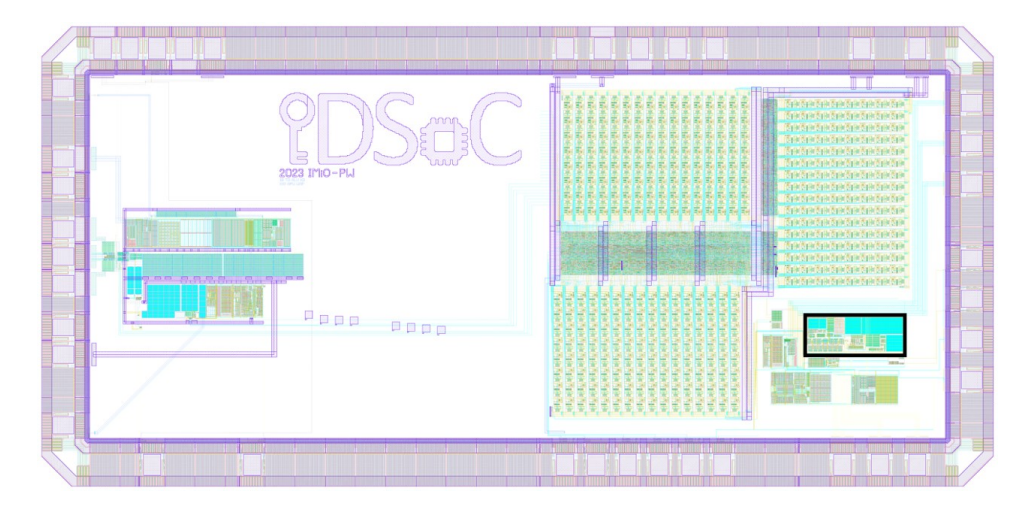


Fig. 21. Chip's masks topography.

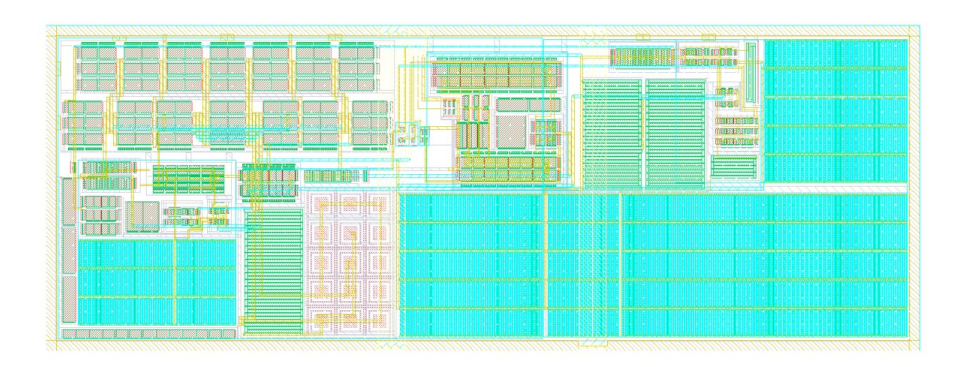


Fig. 22. Temperature sensor layout.

TABLE III
COMPARISON OF RESULTS BETWEEN DIFFERENT IMPLEMENTATIONS.

	[2]	[3]	[4]	[5]	Sim X-FAB	Sim HHGrace	Measurement
Node [nm]	65	180	65	180	180	90	180
Area [mm ²]	0.0082	0.09	0.044	0.45	0.04	0.03	0.04
Supply [V]	0.85 - 1.05	1.2	0.6 - 1.2	3	2.8 - 3.8	2.8 - 3.8	3.3
Temp. Range [°C]	0 - 100	0 - 100	-45 - 85	0 - 100	-40 - 120	-40 - 120	-40 - 120
Accuracy [°C]	0.9	1.5	4	1.33	0.44	0.8	1.37
Power [µW]	135.3	0.071	47.2	0.075	300	135	300

the temperature sensor was implemented in HHgrace 90 nm CMOS technology, and calibration procedure was performed based on simulation results. Results confirmed that the method gives similar results in both technologies. Table III provides a comparison between the presented design (including simulation and measurement results) and known implementations found in the literature. Further works will focus on verifying the approach in modern technology nodes where short-channel effects play more important role and device physics differ, as it is in the case of FD-SOI and FinFet technologies.

REFERENCES

- [1] R. J. Baker, CMOS circuit design, layout, and simulation. Hoboken, New Jersey: John Wiley, 2019.
- [2] T. Anand, K. A. A. Makinwa, and P. K. Hanumolu, "A vco based highly digital temperature sensor with 0.034 °c/mv supply sensitivity," in *IEEE J. Solid-State Circuits*, vol. 51, no. 11, 2016, p. 2651–2663.
- J. Solid-State Circuits, vol. 51, no. 11, 2016, p. 2651–2663.

 [3] S. Jeong, Z. Foo, Y. Lee, J. Y. Sim, D. Blaauw, and D. Sylvester, "A fully-integrated 71 nw cmos temperature sensor for low power wireless sensor nodes," in *IEEE J. Solid-State Circuits*, vol. 49, no. 8, 2014, pp. 1682–1693.
- [4] H. Park and J. Kim, "A 0.8-v resistor-based temperature sensor in 65-nm cmos with supply sensitivity of 0.28 °c/v," in *IEEE J. Solid-State Circuits*, vol. 53, no. 3, 2018, p. 906–912.
- [5] X. Wang, P.-H. P. Wang, Y. Cao, and P. P. Mercier, "A vco based highly digital temperature sensor with 0.034 °c/mv supply sensitivity," in *IEEE Trans. Circuits Syst. I*, vol. 64, no. 9, 2017, p. 2274–2283.